Glass-to-cryogenic-liquid transitions in aqueous solutions suggested by crack healing

Chae Un Kim[a,b,1], Mark W. Tate[c], and Sol M. Gruner[a,c,d,e]

[a]Cornell High Energy Synchrotron Source (CHESS) and Macromolecular Diffraction Facility at CHESS (MacCHESS), Cornell University, Ithaca, NY 14853; [b]Department of Physics, Ulsan National Institute of Science and Technology, Ulsan 689-798, Republic of Korea; [c]Laboratory of Atomic and Solid State Physics, Cornell University, Ithaca, NY 14853; [d]Department of Physics, Cornell University, Ithaca, NY 14853; and [e]Kavli Institute at Cornell for Nanoscale Science, Cornell University, Ithaca, NY 14853

Edited by Pablo G. Debenedetti, Princeton University, Princeton, NJ, and approved July 31, 2015 (received for review May 25, 2015)

Observation of theorized glass-to-liquid transitions between low-density amorphous (LDA) and high-density amorphous (HDA) water states had been stymied by rapid crystallization below the homogeneous water nucleation temperature (~235 K at 0.1 MPa). We report optical and X-ray observations suggestive of glass-to-liquid transitions in these states. Crack healing, indicative of liquid, occurs when LDA ice transforms to cubic ice at 160 K, and when HDA ice transforms to the LDA state at temperatures as low as 120 K. X-ray diffraction study of the HDA to LDA transition clearly shows the characteristics of a first-order transition. Study of the glass-to-liquid transitions in nanoconfined aqueous solutions shows them to be independent of the solute concentrations, suggesting that they represent an intrinsic property of water. These findings support theories that LDA and HDA ice are thermodynamically distinct and that they are continuously connected to two different liquid states of water.

glass-to-liquid transition | high-density amorphous ice | low-density amorphous ice | quenched HDA | first-order phase transition

Water has glassy states, including low-density amorphous (LDA) and high-density amorphous (HDA) ice (1–3). The glass-to-liquid transition in these polyamorphic forms of ice is the focus of theories proposed to explain anomalous properties of supercooled water (4–8). Although supporting experimental evidence exists (9–15), it remains controversial as the direct observation of a glass-to-liquid transition has been stymied by rapid crystallization below the homogeneous nucleation temperature (~235 K at 0.1 MPa).

In general, glasses are nonergodic, noncrystalline solids, in which atoms are fixed to their initial positions for macroscopically long periods of time (16). As is well known, when stress is applied, glasses can be cracked. Above the glass transition temperature, T_g, the ergodic liquid is restored, and the stress-induced cracks in glasses can be healed by the diffusive motions of liquids. Indeed, it has been shown that the crack-healing process is reproducible and correlated with the glass transition temperatures, independent of liquid fragility (17, 18).

Results

Bulk Water. In this study, crack healing is used to probe the molecular mobility in cryogenic transitions between glassy states of water or between glassy and crystalline states. Cracks do not heal for a sample held within any particular cryogenic solid state, indicating a low mobility in each of these states. Crack healing observed during phase transformations requires a high molecular mobility and is suggestive of an intermediate glass-to-liquid transition in the pathway between solid states. Fig. 1 shows the paths in a schematic phase diagram of water that were used to form and probe LDA and HDA ice. To facilitate vitrification of the bulk state of water, either NaK tartrate [sodium potassium tartrate, 0.9 M; mole fraction (moles salt/total moles) of 0.016 or hydration number R (moles H_2O/moles salt) of 62] or NaCl (sodium chloride, 1.5 M; mole fraction of 0.027 or R of 37) were added. Although salt additives in water are known to perturb the structure (19–23) and glass-forming properties (24, 25) of water, insight on the thermodynamic properties of pure water has been obtained from aqueous solutions (6, 26–28).

Fig. 2*A* shows crack healing observed during warming of a NaK tartrate (0.9 M) aqueous solution prepared in the LDA state. Cracks made by flexing the LDA sample in a plastic capillary at liquid nitrogen temperature remain intact until 155 K. Above 155 K, cracks begin to heal (Movie S1). In situ X-ray diffraction (Fig. 2*D*) shows that the sample is in the LDA state until 155 K, above which it transforms to cubic ice. Fig. 2 *B* and *C* show crack healing observed during warming of 0.9 M NaK tartrate (Fig. 2*B*) and 1.5 M NaCl (Fig. 2*C*) solutions prepared in the HDA state (Movies S2–S5). In both cases, crack healing is observed beginning at 120 K. In situ X-ray diffraction (Fig. 2 *E*–*G*) shows that crack healing is correlated with the initiation of the phase transition from the HDA to the LDA state. Note that other studies have, instead, observed additional cracking occurring upon phase transformation (29), likely due to higher heating rates, lack of tube confinement which might suppress rapid sample volume expansion, or different methods of sample preparation (30–33).

Fig. 3 shows the time-resolved X-ray diffraction of a 1.5 M NaCl solution undergoing a phase transformation from the HDA to the LDA state at several fixed temperatures. Samples were ramped from 80 K to either 120, 130 , or 140 K at the rate of 6 K/min. X-ray diffraction data were collected immediately after reaching the final temperatures. Fig. 3 *A*–*C* shows the time evolution of the water diffuse diffraction (WDD, Fig. S2*A*) profiles of a 1.5 M NaCl solution during the HDA to LDA transition at 120, 130, and 140 K. The superposition of WDD profiles shows apparent

Significance

For decades, physicists, physical chemists, and biologists have been tremendously intrigued by the unusual thermodynamic and kinetic properties of supercooled water. Theories have been proposed to account for the properties but these theories remain contentious for lack of experimental evidence. We investigated phase behavior of water at cryogenic temperatures and showed clear experimental evidence that the two cryogenic glassy states of water (high-density amorphous and low-density amorphous) undergo glass-to-cryogenic-liquid transitions and they are thermodynamically separated by a first-order phase transition. The results provide insight into the physical origin of the anomalous properties of supercooled water.

Author contributions: C.U.K. and S.M.G. designed research; C.U.K. performed research; C.U.K. and M.W.T. analyzed data; and C.U.K., M.W.T., and S.M.G. wrote the paper.

The authors declare no conflict of interest.

This article is a PNAS Direct Submission.

[1]To whom correspondence should be addressed. Email: cukim@unist.ac.kr.

This article contains supporting information online at www.pnas.org/lookup/suppl/doi:10.1073/pnas.1510256112/-/DCSupplemental.

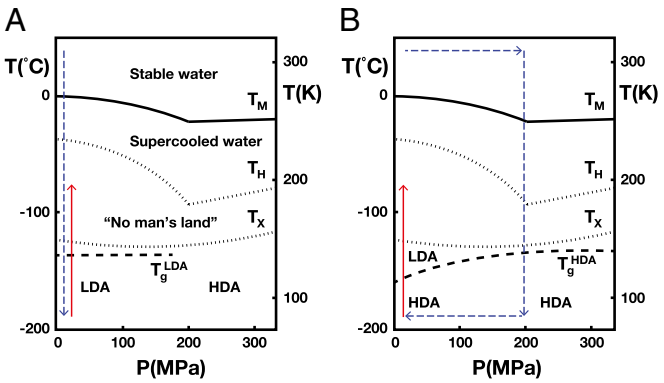

Fig. 1. Phase diagram of noncrystalline water (adapted from ref. 7 with permission from the PCCP Owner Societies) and preparation paths of LDA and HDA. T_M: melting temperature, T_H: homogeneous nucleation temperature, T_X: crystallization temperature. Cooling paths are shown by dashed blue lines and warming paths by red lines. (*A*) LDA ice can be induced by very quickly cryocooling aqueous solutions directly in liquid nitrogen at ambient pressure. Upon warming, LDA ice transforms to crystalline ice phases above T_X in "no man's land," where spontaneous water crystallization cannot be avoided (Figs. S2*A* and S4*A*). T_g^{LDA} is the glass transition temperature of LDA ice. Note that the LDA ice nanoconfined in a protein crystal is induced by this path. (*B*) The HDA ice from both bulk and nanoconfined states of aqueous solutions is induced by cryocooling aqueous solutions at hydrostatic high pressure, 200 MPa. When pressure is released, HDA is metastable at ambient pressure and at liquid nitrogen temperature. Upon warming, HDA first transforms to LDA ice, and then to crystalline ice phases in no man's land (Figs. S2 *B* and *C* and S4 *B* and *C*). T_g^{HDA} is the glass transition temperature of HDA ice (data from ref. 13). Note that the LDA ice of bulk aqueous solution is formed by warming HDA ice at ambient pressure, because crystallization could not be prevented in the dilute solutions upon cooling at ambient pressure (*Supporting Information*).

isosbestic points. A singular value decomposition (SVD) analysis reveals that the WDD profiles can be mostly reconstructed with two major independent states (*Supporting Information*). This result suggests that the intermediate states during the phase transition can be expressed as a coexistence of high-density and low-density states, consistent with a first-order phase transition (29–31, 34–37). Note that the small-angle X-ray scattering (SAXS) region ($Q = 0.3–0.7$ Å^{-1}) in the WDD profiles is initially low in the HDA state and gradually rises during the phase transition, indicating the structural homogeneity of HDA ice (38), increased density fluctuations during the conversion to LDA, and the structural inhomogeneity of LDA ice (21, 22, 28). This is consistent with an interpretation in which the low-density state emerges within a high-density matrix during the HDA to LDA transition (1).

Time evolution of the primary WDD peak position (Fig. 3*D*) was further analyzed to investigate the characteristics of the phase transition from an HDA to an LDA state. The primary WDD peak position is mainly attributed to the O–O correlation in water; hence, it reflects the density of amorphous water. HDA is observed to transform to LDA at each fixed temperature but at different rates. At 120 K the HDA to LDA conversion is still progressing even after ~2 h, at 130 K the transition is almost complete in ~ 1 h, and at 140 K the transition completes in less than 20 min. The time evolution of the phase transition can be fitted with an Avrami–Kolmogorov equation (1), which describes nucleation and growth of a low-density state within a high-density matrix. The Avrami–Kolmogorov fitting suggests that the HDA state completely transforms to the LDA state at these fixed temperatures given sufficient equilibration time (*Supporting Information*). This result indicates that there is density discontinuity between the high-density and low-density states in thermodynamic equilibrium and supports the conclusion that the HDA to LDA transition involves a first-order phase transition rather than a structural relaxation.

Nanoconfined Water. The data shown above were collected from bulk aqueous solutions. Further insight can be obtained from observation of confined water (39). It has been shown that LDA and HDA states of water can be formed inside the ~2–4-nm solvent channels that typically riddle protein crystals by cryocooling at either ambient pressure (for LDA) or high pressure (for HDA) (32) (Fig. 1 and *Supporting Information*). Although nanoconfinement in protein crystals may shift phase boundaries and change dynamics from that of bulk state of water, it has been shown that the confined water undergoes the same phase transitions as bulk water upon warming, exhibiting HDA, LDA, cubic, and hexagonal ice phases (32) (*Supporting Information*). Notably, upon cryocooling, the formation of crystalline forms of ice tends to be suppressed within the nanochannels of the crystal, favoring instead the formation of the amorphous forms of ice. Therefore, the concentration of chemical additives needed for water vitrification in bulk solutions can be reduced or even eliminated. Water dynamics can also be probed by monitoring changes to the crystalline packing of the protein molecules which may occur along with water phase transitions inside the crystals (40).

Fig. 4*A* shows the phase behavior of the LDA state of 0.9 M NaK tartrate and 2.7 M glycerol solution (mole fraction of 0.058) inside a protein crystal along with the resultant protein molecular responses. Similar to that observed for the bulk 0.9 M NaK tartrate solution (Fig. 2*D*), an initial LDA state of the aqueous solution inside the protein crystal transforms to cubic ice when warmed above 160 K (Fig. 4*A*, *Inset*). The protein crystallographic data show that the crystal unit cell parameters expand isotropically with temperature when protein molecules are deep cryocooled into the LDA state and then heated to 160 K. At higher temperatures the crystallographic axes show divergence in the rate of expansion. This anisotropic divergence indicates an onset of rearrangement of the protein molecules inside the crystals, suggesting that the molecules are imbedded in a flexible environment.

Fig. 4*B* shows the phase behavior of an initial HDA state of 0.9 M NaK tartrate solution inside a protein crystal and the resultant protein molecular response. As for the bulk aqueous solutions (Fig. 2 *E* and *F*), the HDA state transforms to LDA ice when warmed above 120 K. The protein crystallographic data show that the crystal unit cell parameters diverge in their expansion rates above 120 K, and that the divergence is correlated with the HDA to LDA transition. Fig. 4 *C* and *D* shows the effect of chemical additives on the phase behavior of the HDA state upon warming inside a protein crystal. As NaK tartrate concentration is reduced to 0.45 M and again to 0 M, the phase transition shifts to lower temperatures overall. However, the divergence in the unit cell parameters is preserved and still correlates with the HDA to LDA transition.

Discussion

We observe crack healing in bulk aqueous solutions and the onset of molecular rearrangement in protein crystals when LDA transforms to cubic ice, both of which require substantial movement of the water molecules. This is consistent with, although not proof of, a liquid-like component arising from the LDA state. This is also consistent with previous reports that LDA ice undergoes a glass-to-liquid transition before transforming to a crystalline ice state (10, 11, 14). Similar crack healing and molecular rearrangements are observed during the HDA to LDA conversion. This result is consistent with the existence of a liquid-like component arising from the HDA state during the HDA to LDA conversion. This result is also consistent with calorimetric and volumetric studies that suggest the existence of a glass-to-liquid transition of HDA ice before transforming to LDA ice (13, 14). The possibility of a liquid-like

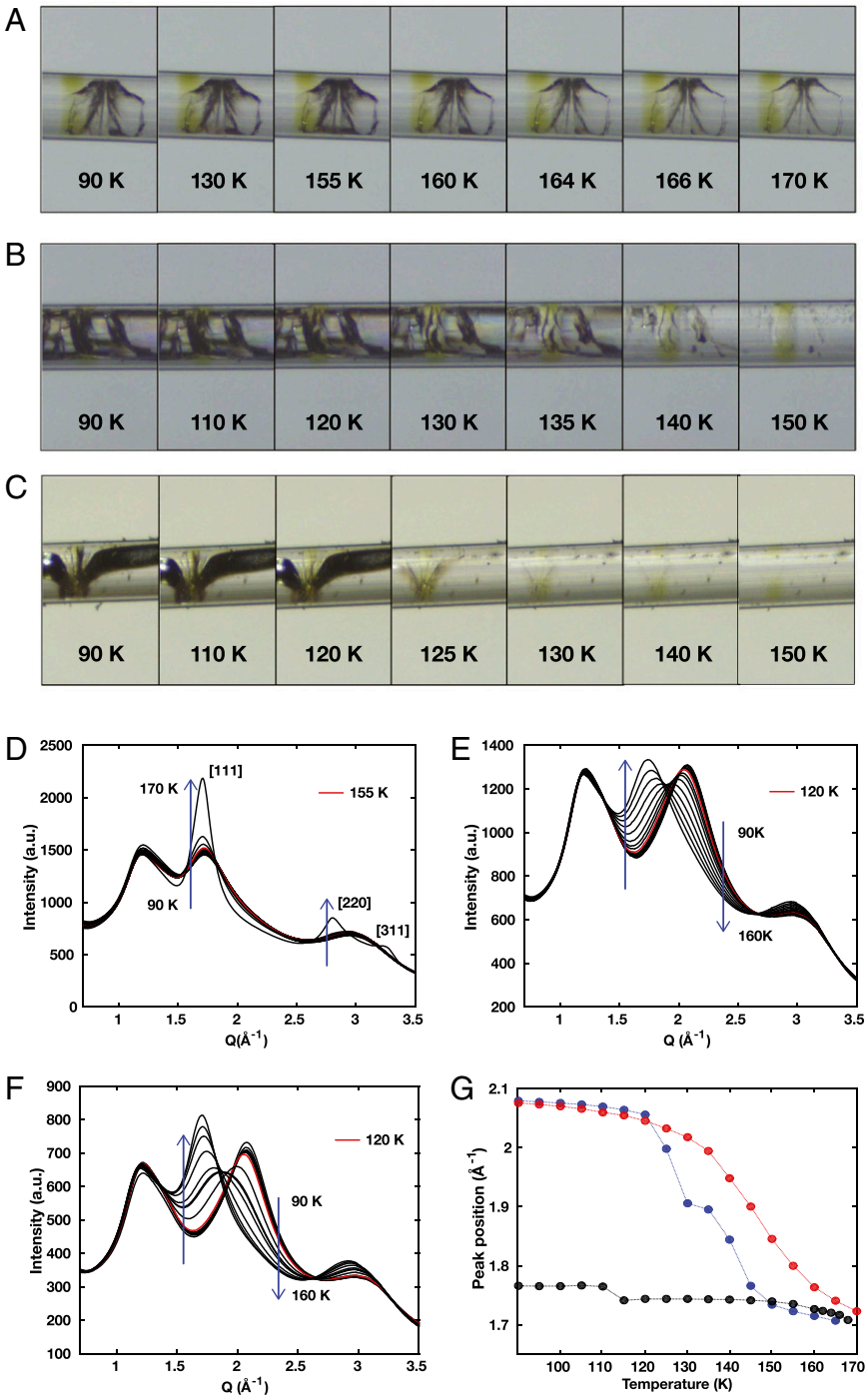

Fig. 2. Correlation between crack healing and phase transitions of LDA and HDA states upon warming. (*A*) Crack healing within the 0.9 M NaK tartrate solution prepared in the LDA state is observed to begin just above 155 K. (*B*) The beginning of crack healing within the 0.9 M NaK tartrate solution prepared in the HDA state is shifted to a lower temperature, 120 K. (*C*) Crack healing within the 1.5 M NaCl solution prepared in the HDA state is also observed around 120 K. (*D–F*) In situ X-ray diffraction profiles during warming of LDA and HDA states of aqueous solutions. (*D*) The LDA ice of the 0.9 M NaK tartrate solution in *A* transforms to the cubic ice phase above 155 K (plotted in red). (*E*) The HDA state of the 0.9 M NaK tartrate solution in *B* transforms to LDA ice above 120 K (plotted in red). (*F*) The HDA state of 1.5 M NaCl solution in *C* transforms to LDA ice above 120 K (plotted in red). The peak around Q = 1.2 Å^{-1} is from the polycarbonate capillary and is almost temperature invariant. (*G*) The position of the primary WDD peak is plotted for the data shown in *D–F*. The peak position of the 0.9 M NaK tartrate solution prepared in the LDA state (black) varies little with temperature, whereas the HDA ice preparation of the 0.9 M NaK tartrate solution (red), and the HDA ice of the 1.5 M NaCl solution (blue) show a marked change as they transform to LDA ice above 120 K. See Fig. S1 for the extra features in the HDA–LDA transition of 1.5 M NaCl solution.

state is further supported by the observation that protein molecules exhibit dynamical fluctuations even at 110 K during the HDA to LDA transition (41). Note that, for the study of water in the bulk state, addition of solutes to the water is necessary to induce the LDA or HDA states without crystallization. On the other hand, our study of water nanoconfined inside protein

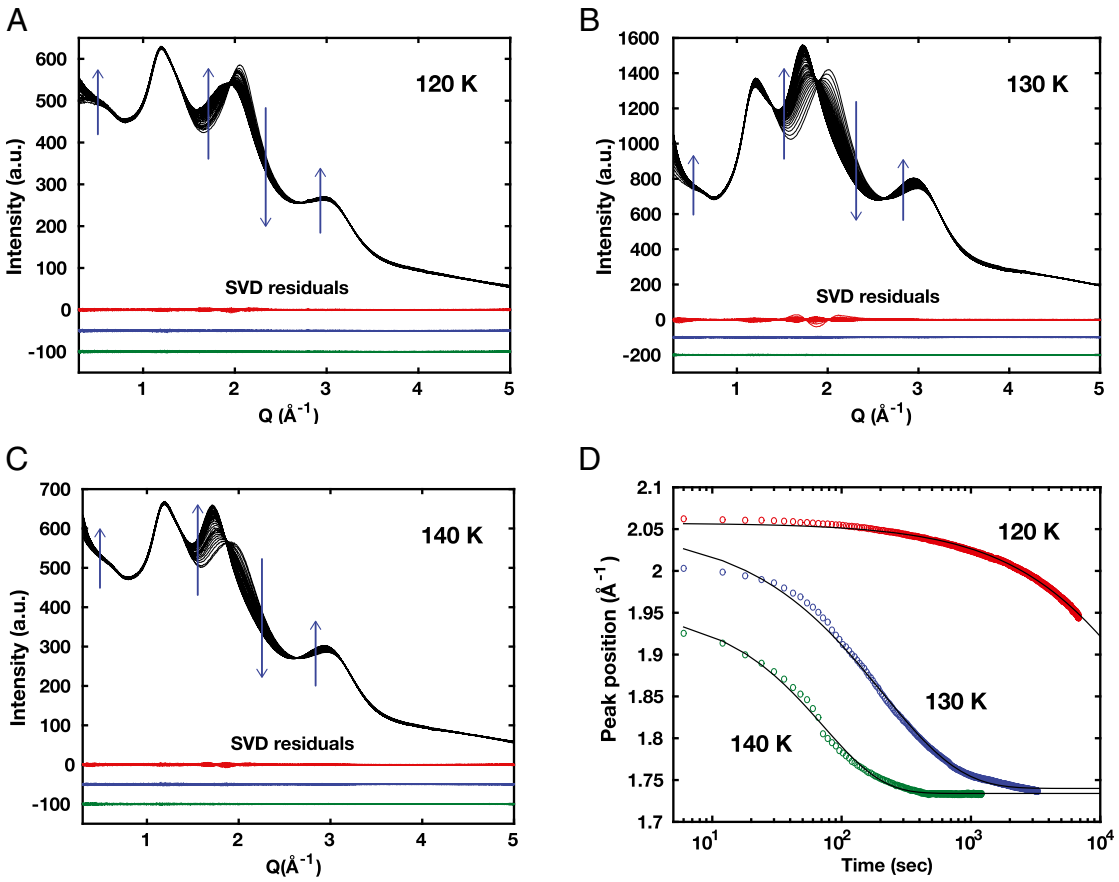

Fig. 3. Time-resolved X-ray diffraction study on the phase transformation of 1.5 M NaCl solution from the HDA to the LDA state at three fixed temperatures. (*A–C*) Selected WDD profiles during the HDA to LDA transition at 120 K (26 profiles), 130 K (39 profiles), and 140 K (32 profiles). Blue arrows indicate the trends for increasing time. Note that SAXS region (Q = 0.3–0.7 Å^{-1}) rises when HDA transforms to the LDA state. Residuals between the experimental profiles and SVD reconstructions are shown for two state reconstructions (red), three state reconstructions (blue, shifted down for visual clarity), and four state reconstructions (green, shifted down for clarity). The peak around Q = 1.2 Å^{-1} is from the polycarbonate capillary. (*D*) Primary WDD peak positions over time when HDA samples are warmed from 80 K at 6 K/min and then equilibrated at 120 K (red), 130 K (blue), and 140 K (green). The data fitted to Avrami–Kolmogorov equations (black solid lines) show that the HDA state progresses to the LDA state (Q = 1.7–1.75 Å^{-1}) at fixed temperatures (Table S1).

crystals does not require the addition of solutes. Although complications can be involved in the interpretations of aqueous solutions and nanoconfined water, our interpretation is that the glass-to-liquid transition of HDA state observed both in the aqueous solutions and in the nanoconfined water is due to the intrinsic properties of water.

Time-resolved X-ray diffraction supports the suggestion that the HDA–LDA transition involves a first-order phase transition. Note that X-ray diffraction produces the same diffraction profile with either a liquid or glassy state of water if the time-averaged internal structures are the same. Hence, the observed first-order phase transition is compatible with a coexisting liquid state of water during the HDA–LDA transition if this liquid is the counterpart of a glassy state of water.

Our results are consistent with the following phase behavior of amorphous water at cryogenic temperatures: When the HDA state is warmed at ambient pressure, it first transforms to a high-density liquid (HDL) state above the glass transition temperature of the HDA state (T_g^{HDA}). This HDL is metastable at ambient pressure and cryogenic temperatures, and must transform to a more stable form of water. Above T_g^{HDA} but below the glass transition temperature of LDA ice (T_g^{LDA}) (Fig. 1), HDL does not crystallize but rather ends up transforming to an LDA state. The time-resolved X-ray diffraction study suggests that HDL either undergoes a nonequilibrium first-order phase transition to LDA or it first undergoes a nonequilibrium first-order phase transition to the liquid counterpart (low-density liquid: LDL) of LDA, then the LDL transforms to LDA. If the latter scenario is correct, our results suggest that the first-order phase transition observed between the HDA and LDA is actually occurring between HDL and LDL, and furthermore the HDL–LDL transition of water at cryogenic temperatures might be directly experimentally approachable during the HDA to LDA transition at ambient pressure. We also want to mention that a liquid state of water during the HDA–LDA transition would open a new experimental regime to investigate water–protein interactions at cryogenic temperatures, thereby providing insight into the physical origin of water-mediated protein dynamics (42).

Note that the HDA ice that has been most widely studied is prepared by pressure-induced amorphization of hexagonal ice at 77 K (43). Depending on the postannealing process, the HDA ice can be further divided into the unannealed HDA (uHDA) and the annealed or expanded HDA (eHDA) (2, 30). Upon warming, uHDA directly transforms to LDA but eHDA first undergoes a glass-to-liquid transition before transforming to LDA (14). On the other hand, the HDA ice used for this study is made by directly quenching normal liquid water to 77 K under pressure (32, 33, 44). This HDA (named quenched HDA or qHDA) shows a glass-to-liquid transition before transforming to LDA. Further studies are needed to probe similarities and differences between qHDA and the other forms of HDAs.

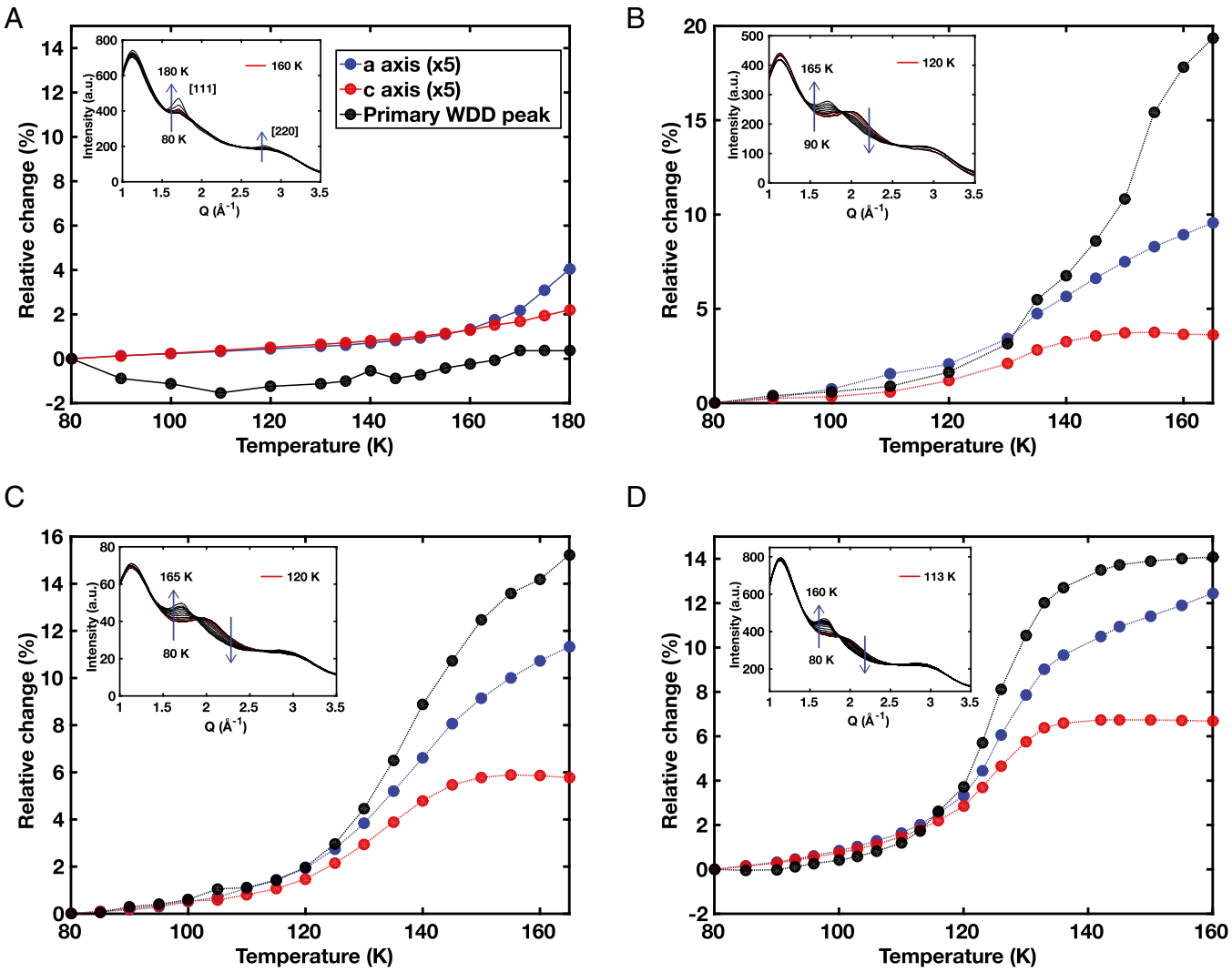

Fig. 4. X-ray diffraction of the phase behavior of water inside a protein crystal and the resulting behavior of the crystal. Change in crystal unit cell parameters [a = b axis (blue); c axis (red)] are plotted as temperature is raised. Changes in primary WDD peak positions (in d spacing, d = 4π/Q) are plotted as an indicator of a water phase transition (black). The changes in the unit cell parameters are magnified 5× for comparison with the changes in the primary WDD peak positions. (*A*) A protein crystal containing 0.9 M NaK tartrate and 2.7 M glycerol is cryocooled at ambient pressure with LDA ice induced internally. Upon warming, the a = b and c axes expand almost isotropically up to 160 K but show divergence in the expansion rates above 160 K. The WDD profiles (*Inset*) show that LDA transforms to cubic ice above 160 K (profile marked in red). (*B–D*) Protein crystals containing 0.9 M NaK tartrate, 0.45 M NaK tartrate, and deionized water are cryocooled at high pressure (200 MPa). Upon warming, the unit cell parameters begin to diverge with different expansion rates at the onset of the transformation from HDA to LDA, beginning at 120–130 K depending on the NaK tartrate concentration. The WDD profiles (*Inset*) show that HDA state begins to transform to the LDA state at 113–120 K (profile marked in red).

Methods

Bulk aqueous solutions were held in polycarbonate capillaries and were cryocooled to liquid nitrogen temperature (77 K) at high pressure (200 MPa) to produce HDA ice. The bulk state of LDA ice was induced by annealing HDA ice at 145 K at ambient pressure, then cooling to 77 K. Cracks were induced by bending the capillaries in liquid nitrogen before loading into the X-ray apparatus. Crack healing was observed by optical microscopy. In situ and time-resolved X-ray diffraction data of bulk solutions were collected at the Cornell High Energy Synchrotron Source (CHESS). To study water confined in protein crystals, thaumatin crystals from *Thaumatococcus daniellii* were used. By volume, a thaumatin crystal consists of 55–60% of water and 40–45% of protein molecules. Protein crystals were cryocooled to 77 K at either ambient pressure or high pressure (200 MPa), to induce LDA and HDA ice, respectively. To obtain unit cell parameters, complete crystallographic data sets were collected at CHESS and analyzed. Further details of methods are available in the *Supporting Information*.

ACKNOWLEDGMENTS. We thank Marian Szebenyi, Abraham Stroock, Markus Seidl, and Thomas Loerting for useful comments and discussions, CHESS staff for support in data collection, and Jinkyun Kim and Ji-Won Park for assistance in manuscript preparation. This work is based upon research conducted at CHESS. CHESS is supported by the National Science Foundation (NSF) and NIH/NIGMS via NSF Award DMR-1332208, and the Macromolecular Diffraction Facility at CHESS resource is supported by National Institute of General Medical Sciences (NIGMS) Award GM103485. This research was supported by the Basic Science Program through the National Research Foundation of Korea funded by the Ministry of Science, ICT and Future Planning (2014R1A2A1A11051254).

1. Koza MM, Schober H, Fischer HE, Hansen T, Fujara F (2003) Kinetics of the high- to low-density amorphous water transition. *J Phys Condens Matter* 15(3):321–332.
2. Loerting T, et al. (2011) How many amorphous ices are there? *Phys Chem Chem Phys* 13(19):8783–8794.
3. Soper AK (2008) Structural transformations in amorphous ice and supercooled water and their relevance to the phase diagram of water. *Mol Phys* 106(16-18):2053–2076.
4. Debenedetti PG (2003) Supercooled and glassy water. *J Phys Condens Matter* 15(45): R1669–R1726.

5. Mishima O, Stanley HE (1998) The relationship between liquid, supercooled and glassy water. *Nature* 396(6709):329–335.
6. Angell CA (2008) Insights into phases of liquid water from study of its unusual glass-forming properties. *Science* 319(5863):582–587.
7. Stanley HE, et al. (2000) The puzzling behavior of water at very low temperature. *Phys Chem Chem Phys* 2(8):1551–1558.
8. Poole PH, Sciortino F, Essmann U, Stanley HE (1992) Phase-behavior of metastable water. *Nature* 360(6402):324–328.
9. Andersson O (2011) Glass-liquid transition of water at high pressure. *Proc Natl Acad Sci USA* 108(27):11013–11016.
10. Elsaesser MS, Winkel K, Mayer E, Loerting T (2010) Reversibility and isotope effect of the calorimetric glass–> liquid transition of low-density amorphous ice. *Phys Chem Chem Phys* 12(3):708–712.
11. Johari GP, Hallbrucker A, Mayer E (1987) The glass liquid transition of hyperquenched water. *Nature* 330(6148):552–553.
12. Mishima O (2004) The glass-to-liquid transition of the emulsified high-density amorphous ice made by pressure-induced amorphization. *J Chem Phys* 121(7): 3161–3164.
13. Seidl M, et al. (2011) Volumetric study consistent with a glass-to-liquid transition in amorphous ices under pressure. *Phys Rev B* 83(10):100201.
14. Amann-Winkel K, et al. (2013) Water's second glass transition. *Proc Natl Acad Sci USA* 110(44):17720–17725.
15. Kanno H (1987) Double glass transitions in aqueous lithium-chloride solutions vitrified at high-pressures - evidence for a liquid-liquid immiscibility. *J Phys Chem-Us* 91(7): 1967–1971.
16. Angell CA, Ngai KL, McKenna GB, McMillan PF, Martin SW (2000) Relaxation in glassforming liquids and amorphous solids. *J Appl Phys* 88(6):3113–3157.
17. Wu WH, et al. (2008) A method to study the crack healing process of glassformers. *Appl Phys Lett* 92(1):011918.
18. Zhang JL, Wu WH, Zhou HW, Guo XZ, Huang YN (2008) Obtaining the glass transition temperature by measuring the crack healing process of glassformers. *Appl Phys Lett* 92(13):131906.
19. Leberman R, Soper AK (1995) Effect of high salt concentrations on water structure. *Nature* 378(6555):364–366.
20. Winkel K, et al. (2011) Structural study of low concentration LiCl aqueous solutions in the liquid, supercooled, and hyperquenched glassy states. *J Chem Phys* 134(2):024515.
21. Suzuki Y, Mishima O (2000) Two distinct Raman profiles of glassy dilute LiCl solution. *Phys Rev Lett* 85(6):1322–1325.
22. Le L, Molinero V (2011) Nanophase segregation in supercooled aqueous solutions and their glasses driven by the polyamorphism of water. *J Phys Chem A* 115(23): 5900–5907.
23. Bove LE, Klotz S, Philippe J, Saitta AM (2011) Pressure-induced polyamorphism in salty water. *Phys Rev Lett* 106(12):125701.
24. Hofer K, Hallbrucker A, Mayer E, Johari GP (1989) Vitrified dilute aqueous-solutions. 3. Plasticization of water's H-bonded network and the glass-transition temperatures minimum. *J Phys Chem* 93(11):4674–4677.
25. Angell CA, Sare EI (1970) Glass-forming composition regions and glass transition temperatures for aqueous electrolyte solutions. *J Chem Phys* 52(3):1058–1068.
26. Mishima O (2007) Phase separation in dilute LiCl-H2O solution related to the polyamorphism of liquid water. *J Chem Phys* 126(24):244507.
27. Kobayashi M, Tanaka H (2011) Possible link of the V-shaped phase diagram to the glass-forming ability and fragility in a water-salt mixture. *Phys Rev Lett* 106(12): 125703.
28. Chatterjee S, Debenedetti PG (2006) Fluid-phase behavior of binary mixtures in which one component can have two critical points. *J Chem Phys* 124(15):154503.
29. Mishima O, Suzuki Y (2002) Propagation of the polyamorphic transition of ice and the liquid-liquid critical point. *Nature* 419(6907):599–603.
30. Nelmes RJ, et al. (2006) Annealed high-density amorphous ice under pressure. *Nat Phys* 2(6):414–418.
31. Winkel K, Mayer E, Loerting T (2011) Equilibrated high-density amorphous ice and its first-order transition to the low-density form. *J Phys Chem B* 115(48):14141–14148.
32. Kim CU, Chen YF, Tate MW, Gruner SM (2008) Pressure-induced high-density amorphous ice in protein crystals. *J Appl Cryst* 41(Pt 1):1–7.
33. Kim CU, Kapfer R, Gruner SM (2005) High-pressure cooling of protein crystals without cryoprotectants. *Acta Crystallogr D Biol Crystallogr* 61(Pt 7):881–890.
34. Mishima O, Calvert LD, Whalley E (1985) An apparently 1st-order transition between 2 amorphous phases of ice induced by pressure. *Nature* 314(6006):76–78.
35. Yoshimura Y, Mao HK, Hemley RJ (2007) In situ Raman spectroscopy of reversible low-temperature transition between low-density and high-density amorphous ices. *J Phys Condens Matter* 19(42):174505.
36. Klotz S, et al. (2005) Nature of the polyamorphic transition in ice under pressure. *Phys Rev Lett* 94(2):025506.
37. Mishima O, Takemura K, Aoki K (1991) Visual observations of the amorphous-amorphous transition in H2O under pressure. *Science* 254(5030):406–408.
38. Kim CU, Wierman JL, Gillilan R, Lima E, Gruner SM (2013) A high-pressure cryocooling method for protein crystals and biological samples with reduced background X-ray scatter. *J Appl Cryst* 46(Pt 1):234–241.
39. Bertrand CE, Zhang Y, Chen SH (2013) Deeply-cooled water under strong confinement: Neutron scattering investigations and the liquid-liquid critical point hypothesis. *Phys Chem Chem Phys* 15(3):721–745.
40. Kim CU, Barstow B, Tate MW, Gruner SM (2009) Evidence for liquid water during the high-density to low-density amorphous ice transition. *Proc Natl Acad Sci USA* 106(12): 4596–4600.
41. Kim CU, Tate MW, Gruner SM (2011) Protein dynamical transition at 110 K. *Proc Natl Acad Sci USA* 108(52):20897–20901.
42. Ringe D, Petsko GA (2003) The 'glass transition' in protein dynamics: What it is, why it occurs, and how to exploit it. *Biophys Chem* 105(2-3):667–680.
43. Mishima O, Calvert LD, Whalley E (1984) Melting Ice-I at 77 K and 10 Kbar - a new method of making amorphous solids. *Nature* 310(5976):393–395.
44. Mishima O, Suzuki Y (2001) Vitrification of emulsified liquid water under pressure. *J Chem Phys* 115(9):4199–4202.
45. Murray BJ, Bertram AK (2006) Formation and stability of cubic ice in water droplets. *Phys Chem Chem Phys* 8(1):186–192.
46. Blackman M, Lisgarten ND (1957) The cubic and other structural forms of ice at low temperature and pressure. *Proc R Soc London, Ser A* 239(1216):93–107.
47. Handle PH, Seidl M, Loerting T (2012) Relaxation time of high-density amorphous ice. *Phys Rev Lett* 108(22):225901.
48. Ko TP, Day J, Greenwood A, McPherson A (1994) Structures of three crystal forms of the sweet protein thaumatin. *Acta Crystallogr D Biol Crystallogr* 50(Pt 6):813–825.
49. Otwinowski Z, Minor W (1997) Processing of X-ray diffraction data collected in oscillation mode. *Methods Enzymol* 276:307–326.

Supporting Information

Kim et al. 10.1073/pnas.1510256112

Experimental Details for the Study on the Aqueous Solutions in Bulk State

Sample Preparation. NaK tartrate (0.9 M) and NaCl (1.5 M) solutions were used for the study on the bulk state of water. The solution was inserted into a polycarbonate capillary having a length of 15 mm, an inner diameter of 200 μm, and a wall thickness of 50 μm.

Sample Cryocooling. To induce HDA ice, capillary samples containing 0.9 M NaK tartrate or 1.5 M NaCl solution were cryocooled at high pressure as described in Kim et al. (33). Briefly, samples were loaded into the high-pressure cryocooling apparatus, which was then pressurized with helium gas to 200 MPa at ambient temperature. Five minutes later, while still at high pressure, the samples were dropped into a zone at liquid-nitrogen temperature. Helium pressure was then released. Thereafter samples were handled and stored at ambient pressure and at liquid nitrogen temperature before crack-healing observation and X-ray diffraction measurements.

To induce LDA ice, the HDA ice produced by high-pressure cryocooling was annealed at 145 K for 1 h and cooled back to 80 K at ambient pressure. The formation of LDA ice was confirmed by X-ray diffraction. Note that LDA ice could not be obtained in the bulk aqueous solution by directly cryocooling at ambient pressure (instead, hexagonal ice was always induced).

Observation of Crack Healing. To induce cracks inside LDA and HDA ice, mechanical stress was applied to the capillary sample by bending it with forceps in liquid nitrogen. Then the sample was loaded on a goniometer on an X-ray beamline (see the next section for details) under a cryogenic N_2 gas stream at 80 K (Cryostream 700 series cryocooler from Oxford Cryosystems). A cryotong (Hampton Research) was used to prevent sample warming during sample loading.

The temperature of a capillary sample was increased at the rate of 6 K/min. At each desired temperature (5-K steps, starting from 80 K), image snapshots were taken through a beamline optical microscope. At the same time, in situ X-ray diffraction data were collected to probe water phases, as described in the next section.

Crack healing was observed when LDA transformed to cubic ice and HDA transformed to LDA upon warming (see Fig. 2 in the main text and Movies S1–S5). Crack healing progressed when HDA transformed to LDA at fixed temperatures, suggesting that crack healing is related to the phase transition of amorphous water rather than temperature changes (Fig. S1).

X-Ray Diffraction Measurement. X-ray diffraction data were collected at the macromolecular crystallography stations A1 (λ = 0.9770 Å, Area Detector Systems Corporation (ADSC) Quantum 210 CCD detector, beam size of 100 μm) and F1 (λ = 0.9179 Å, ADSC Quantum 270 CCD detector, beam size of 100 μm) at CHESS. X-ray diffraction data from the crack-induced samples were collected with temperature steps of 5 K. The distance between the sample and the detector was 200 mm and the X-ray exposure time was 10 s.

A time-resolved X-ray study was performed during the HDA–LDA transition of a 1.5 M NaCl solution at fixed temperatures. Three HDA samples were first loaded at 80 K onto the beamline and then warmed to 120, 130, and 140 K, respectively, at the maximum warming rate (6 K/min). Immediately after reaching the target temperature, X-ray diffraction data were collected. The sample-to-detector distance was 200 mm and the X-ray exposure time was 3 s. Including detector readout and image processing time, 10 X-ray diffraction images were recorded per minute. A total of 1,135 images were collected at 120 K (~2 h), 549 images at 130 K (~1 h), and 203 images at 140 K (~20 min).

The magnitude of the scattering vector Q is given by $Q = (4\pi\sin(\theta))/\lambda$, where λ is the X-ray wavelength and 2θ is the angle between the incident beam and the diffracted X-rays. The corresponding d spacing in real space is given by $d = 2\pi/Q$.

X-ray diffraction images of aqueous solutions in the bulk state during warming are shown in Fig. S2. Note that aqueous solutions in the bulk state undergo the same phase transitions from HDA to LDA, cubic, and hexagonal ice as pure bulk water (11, 34, 45).

X-Ray Data Analysis: Data Processing. The X-ray diffraction data were azimuthally averaged as a function of Q. The sample-to-detector distance was calibrated using the reported peak positions of hexagonal ice (46). Peak positions for the broad diffraction of LDA and HDA ice from the 0.9 M NaK tartrate and 1.5 M NaCl solutions were determined by fitting a series of three Voigt functions (one each for the diffuse peak from the polycarbonate capillary, the primary amorphous ice peak, and a secondary ice peak) with a quadratic background.

The processed water WDD profiles from X-ray diffraction images are shown in Fig. S2.

X-Ray Data Analysis: Time-Resolved Study. The primary WDD peak position in the time-resolved study was fitted to an Avrami–Kolmogorov equation (1):

$$P(t,T) = A\,\exp\left[-(t/\tau(T))^n\right] + P_\infty,$$

where P(t,T) is the primary WDD peak position, t is time, $\tau(T)$ is a temperature (T)-dependent relaxation time, n is a characteristic parameter which reflects the nature of the transformation, and P_∞ is the primary WDD peak position when $t \to \infty$.

The fitting parameters were determined using MATLAB with a 95% confidence bound; they can be found in Table S1.

The fact that P_∞ is the same as the primary WDD peak position of LDA ice (Q = 1.70–1.75 $Å^{-1}$) suggests that the HDA state completely transforms to the LDA state at these fixed temperatures if the HDA state is equilibrated long enough. This is characteristic of a first-order phase transition.

Assuming that the transition is a thermally activated process, the activation energy barrier ΔE can be determined using the Arrhenius equation

$$\tau(T) = \tau_\infty \exp[\Delta E/RT],$$

where R is the gas constant and τ_∞ is the relaxation time when $T \to \infty$. The estimated activation energy ΔE is ~ 40 kJ mol^{-1}.

X-Ray Data Analysis: SVD. If the HDA-to-LDA transition is a first-order phase transition, the WDD profiles of the intermediate states should be expressed as a superposition of two independent states, i.e., initial (HDA) and final (LDA) states.

SVD analysis was performed to obtain the number of independent states needed to reconstruct the WDD profiles. Fig. S3 shows the results of SVD analysis on the WDD profiles of 1.5 M NaCl solution at 130 K. It is apparent that the experimental profiles can be mostly reconstructed using the two major independent states from the SVD analysis. One or two additional

minor states were detected. We estimate that the additional minor states are due to the structural relaxation of amorphous water upon warming (1, 47), and during the glass-to-liquid transition.

Experimental Details for the Study on the Aqueous Solutions Confined in Protein Crystals

Protein Crystallization and Crystal Handling. The protein crystallization method was modified from that described by Ko et al. (48) and was carried out as described by Kim et al. (33). Lyophilized thaumatin powder from *T. daniellii* (catalog no. T7638, Sigma) was used for crystallization without further purification. Crystals were grown at 20 °C by the hanging-drop method, with 25 mg/mL thaumatin solution in 50 mM Hepes buffer at pH 7 and a crystallization solution containing 0.9 M sodium potassium tartrate (NaK tartrate) as a precipitant. The crystal space group was determined to be $P4_12_12$ (a = b = ~58 Å, c = ~150 Å), having a solvent content of 55–60% by volume.

To adjust solvent concentrations in protein crystals, the fully grown thaumatin crystals were equilibrated with 0.9 M, 0.45 M NaK tartrate solutions, and with deionized water (0 M NaK tartrate solution). To reduce osmotic shock, crystals were gradually transferred to the target concentration in 0.1-M steps.

Note that equilibrating protein crystals in deionized water does not necessarily remove all of the chemical solutes in protein crystals. It is still possible that some solute molecules remain in the protein crystals by tightly binding to protein molecules. However, these tightly binding solutes are recorded in the Bragg diffraction in X-ray measurement in the same way that highly ordered water molecules around protein molecules are recorded in the Bragg diffraction. Equilibrating protein crystals in deionized water ensures that there are no solutes freely floating in the solvent channels inside the protein crystals. The solute-free, disordered water molecules in the solvent channel are responsible for the WDD in X-ray diffraction measurement.

Crystal Cryocooling. Before cryocooling of crystals, liquid surrounding the crystals was carefully removed during crystal coating with a mineral oil. The WDD was thus produced almost entirely from the solution inside the crystal. The oil coating also prevented crystal dehydration during cryocooling. To induce HDA ice inside protein crystals, protein crystals containing 0 M to 0.9 M NaK tartrate were cryocooled under high pressure (200 MPa) (33) as in the bulk state of aqueous solution. LDA ice was induced by directly plunging a protein crystal into liquid nitrogen at ambient pressure rather than annealing the pressure-induced HDA ice to 145 K at ambient pressure. This different procedure was because conversion from HDA to LDA seemed to take a much longer time in a protein crystal. The crystals containing only NaK tartrate could not be easily cryocooled to produce LDA ice at ambient pressure (instead, cubic or hexagonal ice formed). Therefore, 2.7 M glycerol was added to the crystal (0.9 M NaK tartrate) to suppress crystallization upon cryocooling.

X-Ray Diffraction Data Collection. The crystallographic X-ray diffraction data were collected at the macromolecular crystallography stations F1 (λ = 0.9179 Å, ADSC Quantum 270 CCD detector, beam size of 100 μm), and F2 (λ = 0.9795 Å, ADSC Quantum 210 CCD detector, beam size of 150 μm) at CHESS. The cryocooled crystals were transferred from liquid nitrogen to a goniometer without sample warming. During data collection, the sample temperature, ranging from 80 to 160 K, was controlled by a Cryostream 700 series cryocooler (Oxford Cryosystems). The sample temperature was raised at the rate of 6 K/min. After reaching a desired temperature, samples were held at the temperature for 3–5 min. The X-ray diffraction data of the protein crystals were collected with temperature steps from 3 to 10 K. At each temperature, two types of data sets were collected. First, to extract the WDD profile, a diffraction image was obtained with 10–15-s exposure time and an oscillation angle of 1°. Then, to obtain unit cell parameters, a complete data set was collected covering 60–90° of crystal rotation. The X-ray exposure time for each frame was 1 s with an oscillation angle of 1°. The data collection parameters were the same for all of the complete datasets from a single crystal.

X-ray diffraction images of protein crystals during warming are shown in Fig. S4. Note that the aqueous solutions confined in protein crystals show the same phase transitions (from HDA to LDA, cubic, and hexagonal ice) as the aqueous solutions in the bulk state (Fig. S2).

X-Ray Data Analysis: WDD from Protein Crystals. Each diffraction pattern from a protein crystal consists of Bragg peaks from the protein molecules in the crystal plus diffuse diffraction rings arising from the oil external to the crystal and water internal to the crystal (Fig. S4). The underlying diffuse diffraction from the diffraction image was isolated from the Bragg spots by applying a custom polar coordinate median filter to the intensity values of the image. The sample-to-detector distance was calibrated based on the known Bragg peaks of hexagonal ice (46). To determine the position of the WDD peak, the median-filtered diffuse scattering curves were fit to a series of three Voigt functions plus linear background: one Voigt function at the position of the oil scattering peak, one at the main WDD peak, and a third function at the secondary WDD peak.

The extracted WDD profiles from protein crystallographic images are shown in Fig. S4.

X-Ray Data Analysis: Crystal Bragg Diffraction. To obtain unit-cell parameters, the complete thaumatin data sets were indexed, integrated, postrefined, and scaled with HKL2000 (49).

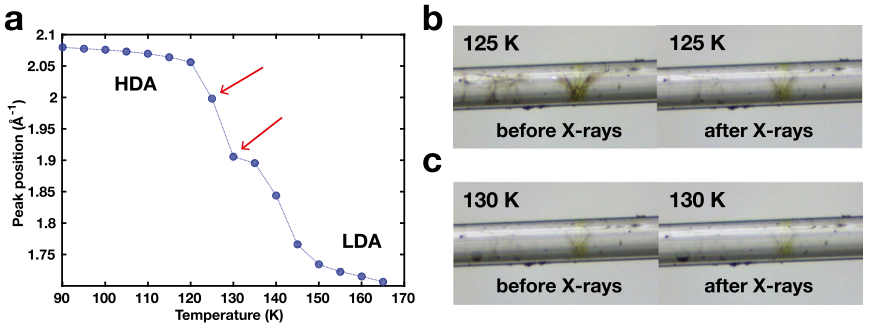

Fig. S1. Progression of crack healing during HDA to LDA transitions at fixed temperatures. (*A*) NaCl solution (1.5 M) was cryocooled at 200 MPa to induce HDA ice. When warmed, HDA ice transforms to LDA ice. At each temperature, a sample image snapshot was taken before X-ray measurement, except for 125 and 130 K (arrows). At 125 and 130 K, two sample image snapshots were taken, before and after X-ray measurement. Note that the primary WDD peak positions at 125 and 130 K are slightly shifted down to lower Q value, from the overall transition profile, due to progression of the HDA to LDA transition during the longer holding time at these temperatures (see Fig. 3 in the main text). (*B* and *C*) Crack healing at 125 and 130 K before and after X-ray measurement. Cracks are progressively healed at these fixed temperatures.

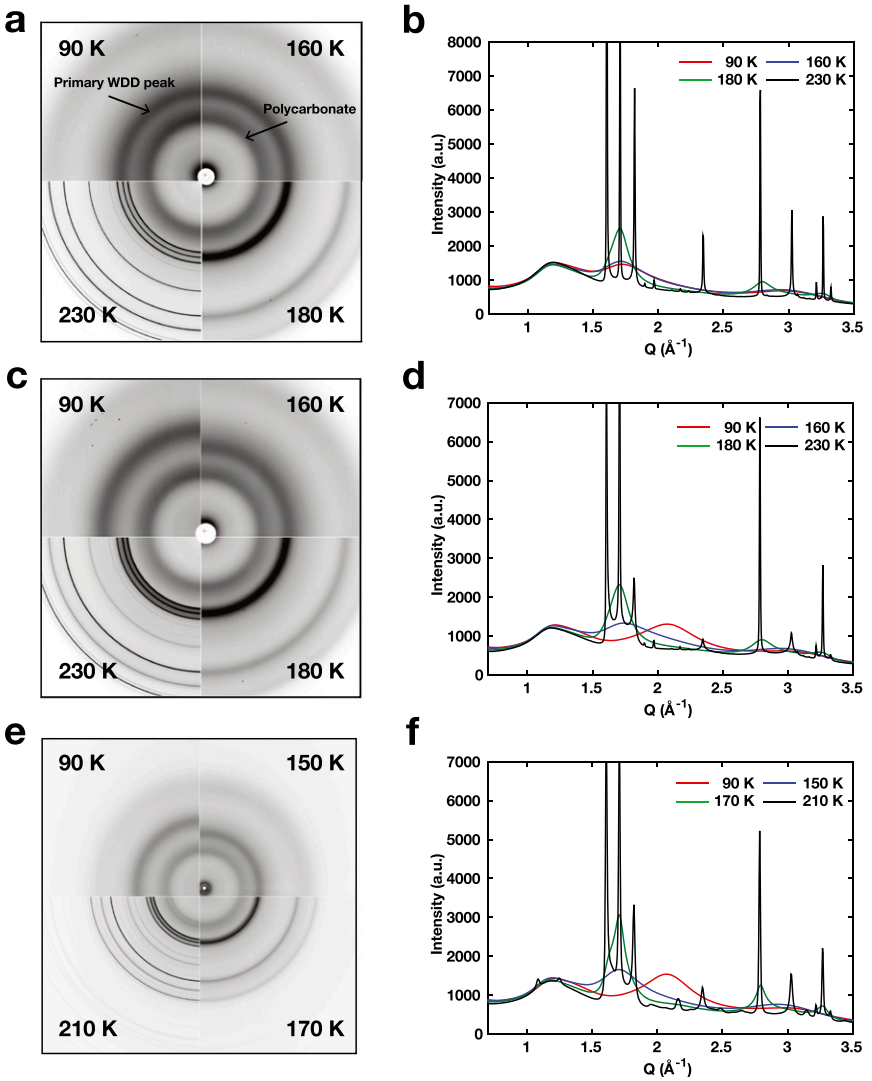

Fig. S2. X-ray diffraction images and corresponding WDD profiles of aqueous solutions in the bulk state during warming. The innermost diffraction ring is from the polycarbonate capillary, and its position is almost temperature invariant. The second innermost diffraction ring is the primary WDD peak of aqueous solution and changes most dramatically during the water phase transition. (*A* and *B*) Phase behavior of the LDA state of 0.9 M NaK tartrate solution during warming. It stays in the LDA state until 160 K and then transforms to cubic and hexagonal ice. (*C* and *D*) Phase behavior of the HDA state of 0.9 M NaK tartrate solution during warming. It transforms to LDA, cubic, and hexagonal phases. (*E* and *F*) Phase behavior of the HDA state of 1.5 M NaCl solution during warming. It transforms to LDA, cubic, and hexagonal phases.

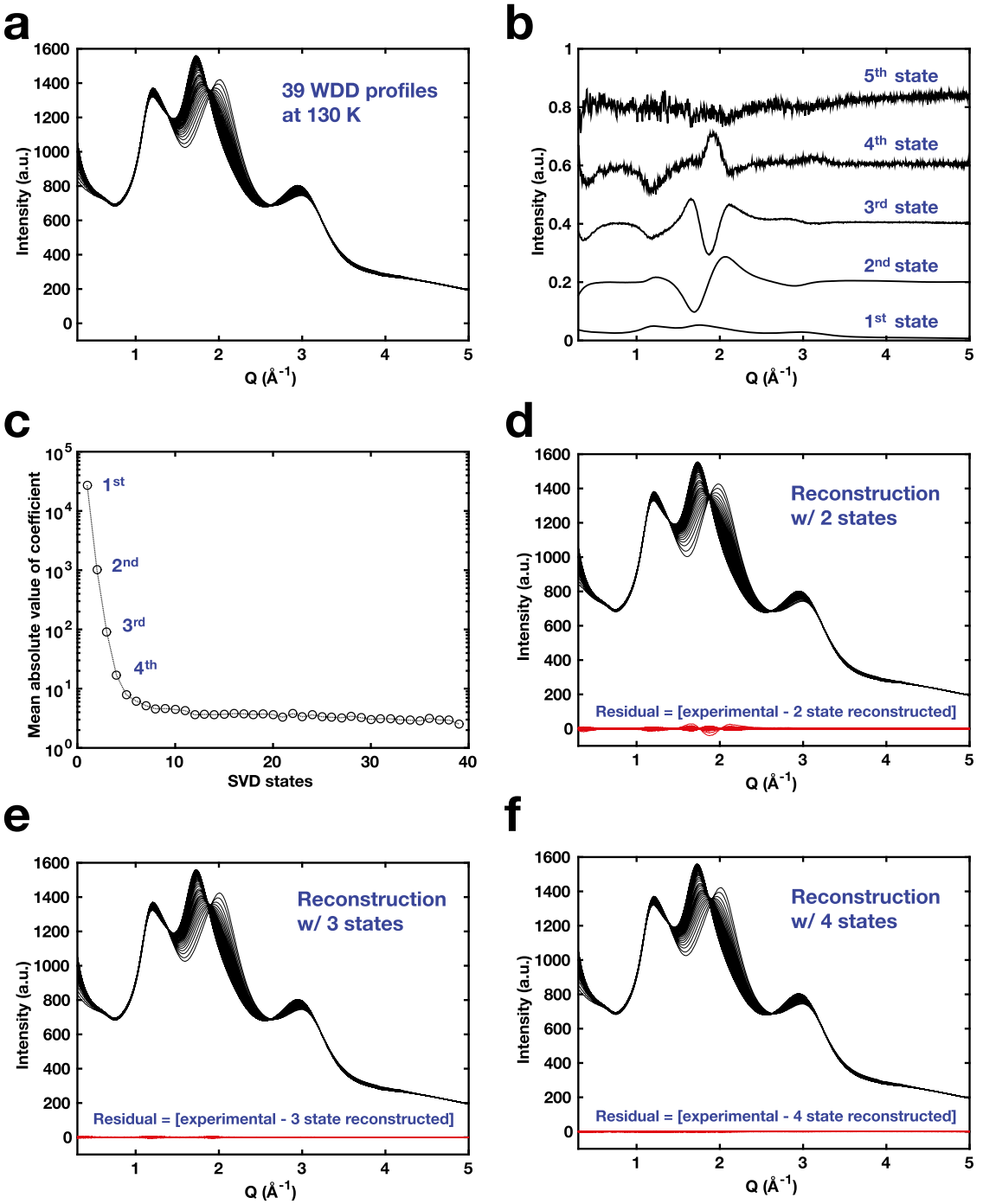

Fig. S3. SVD analysis on the WDD profiles of 1.5 M NaCl solution at 130 K. (*A*) Thirty-nine sequential experimental WDD profiles show a phase transition from HDA to LDA state at 130 K. (*B*) The first five SVD independent states (i.e., state vectors). Each state is shifted up by 0.2 for visual clarity. Note that there are numerous different ways to choose the basis states; each state is purely mathematical and does not necessarily reflect a physically meaningful water phase. (*C*) The mean absolute values of the coefficients for the SVD states show that there are two major states and one or two additional minor states above noise level. (*D–F*) Reconstruction of WDD profiles with two, three, and four primary SVD states, respectively. The residual is calculated by subtracting reconstructed profiles from experimental profiles.

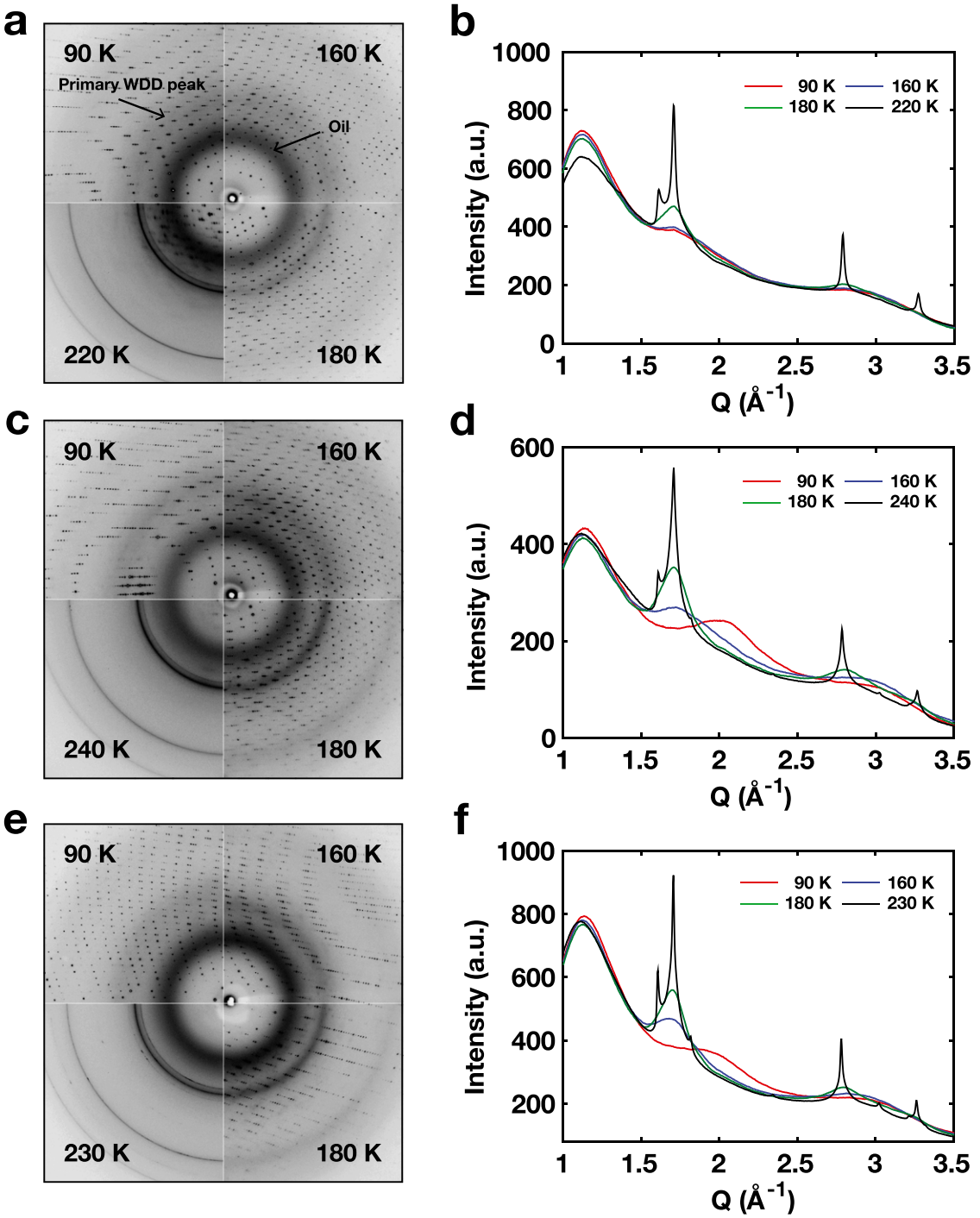

Fig. S4. X-ray diffraction images of protein crystals and extracted WDD profiles of aqueous solution inside protein crystals. The innermost diffraction ring is from a mineral oil, and its position is almost temperature invariant. The second innermost diffraction ring is the primary WDD peak of aqueous solution and changes most dramatically during water phase transitions. (*A* and *B*) Phase behavior of the LDA state of 0.9 M NaK tartrate and 2.7 M glycerol solution inside a protein crystal during warming. It stays in the LDA state until 160 K and then transforms to cubic and hexagonal ice. (*C* and *D*) Phase behavior of the HDA state of 0.9 M NaK tartrate solution inside a protein crystal during warming. It transforms to LDA, cubic, and hexagonal ice phases. (*E* and *F*) Phase behavior of the HDA state of pure water (0 M NaK tartrate) inside a protein crystal during warming. It transforms to LDA, cubic, and hexagonal ice phases.

Table S1. Fitting parameters of the time-resolved X-ray study

	$P(t,T) = A \exp[-(t/\tau(T))^n] + P_\infty$			
Temperature, K	A, $Å^{-1}$	$\tau(T)$, s	n	P_∞, $Å^{-1}$
120	0.317 ± 0.053	(2.21 ± 0.69) × 10^4	0.738 ± 0.026	1.740 ± 0.053
130	0.310 ± 0.005	207.60 ± 5.20	0.715 ± 0.014	1.740 ± 0.005
140	0.219 ± 0.006	72.13 ± 2.81	0.945 ± 0.037	1.734 ± 0.005

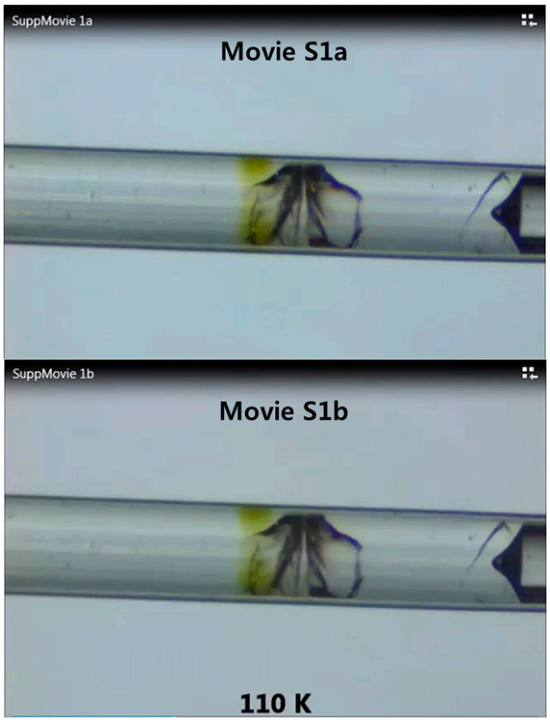

Movie S1. Crack healing in the LDA state of a 0.9 M NaK tartrate solution in a polycarbonate capillary (o.d. = 300 μm, i.d.= 200 μm) during the phase transition of the LDA state to cubic ice. (*A*) Cracks induced in the sample. The sample is rotated by 360° at 90 K to show cracks induced inside. The frame rate used for recording is 7.5 frames per second (fps) and video playback speed is 15 fps. (*B*) Crack healing inside the LDA sample during warming (from 80 to 170 K). Note that crack healing occurs noticeably above 155 K. The image frames are recorded at 5-K increments, and video playback speed is 2 fps.

Movie S1

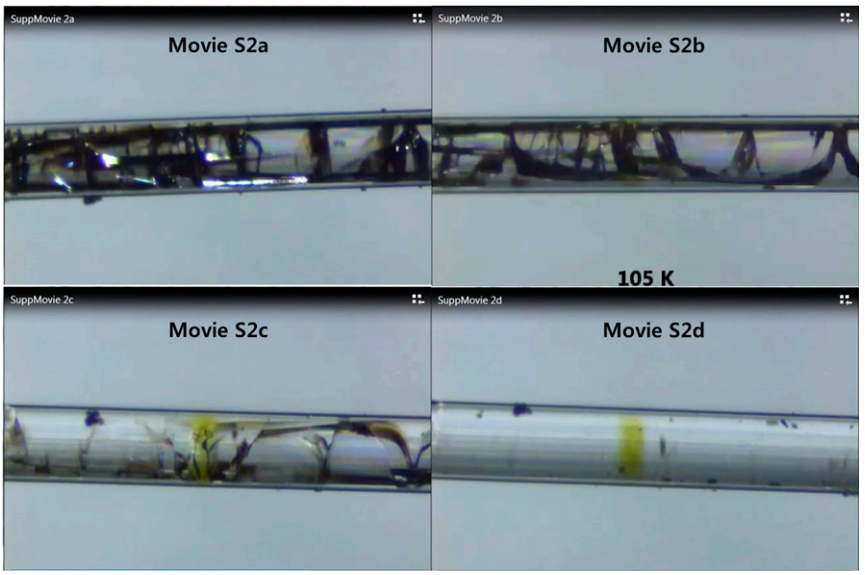

Movie S2. Crack healing in the HDA state of a 0.9 M NaK tartrate solution in a polycarbonate capillary during the transition from the HDA to the LDA state. (*A*) Cracks induced in the sample. The sample is rotated by 360° at 85 K to show cracks induced inside. The frame rate used for recording is 7.5 fps and video playback speed is 15 fps. (*B*) Crack healing inside the HDA sample during warming (from 85 to 160 K). Note that crack healing occurs noticeably above 120 K, which is 35 K lower than in the LDA state (Movie S1). The image frames are recorded every 5 K, and video playback speed is 2 fps. (*C*) Cracks in the sample in the middle of warming. The sample is rotated by 360° at 135 K to show crack healing inside. Note that the cracks observed at 85 K are considerably healed. (*D*) The sample after warming. The sample is rotated by 360° at 160 K to show crack healing inside. Note that the cracks are completely healed.

Movie S2

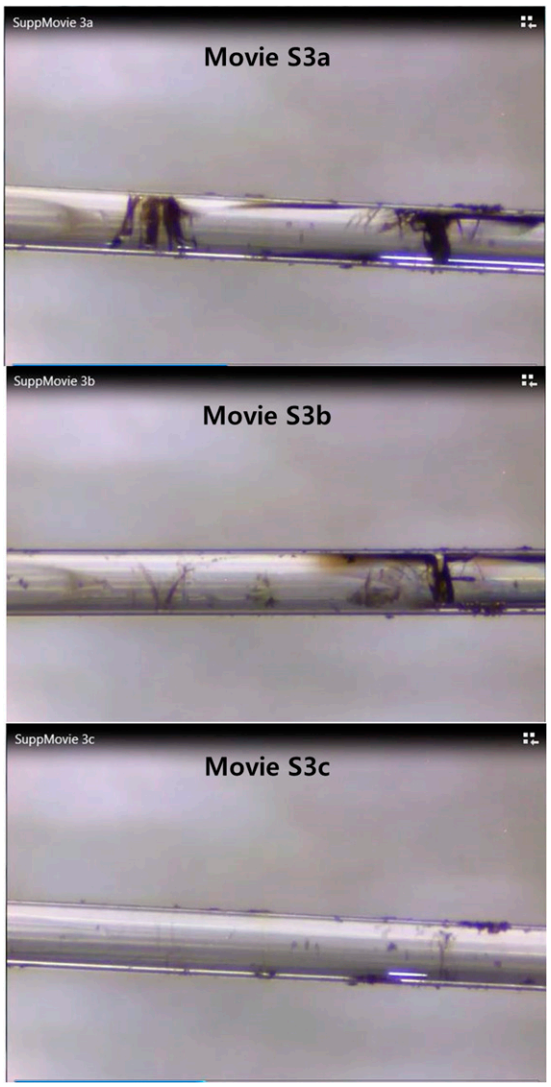

Movie S3. Crack healing in the HDA state of a 0.9 M NaK tartrate solution in a polycarbonate capillary during the phase transition of HDA to LDA state (a different sample from that of Movie S2). (*A*) Cracks induced in the sample. The sample is rotated by 360° at 110 K to show cracks induced inside. The frame rate used for recording is 7.5 fps and video playback speed is 15 fps. (*B*) The HDA sample is continuously recorded during warming from 110 to 150 K. Note that cracks heal completely during warming. The frame rate used for recording is 7.5 fps and video playback speed is 240 fps. (*C*) The sample after warming. The sample is rotated by 360° at 150 K.

Movie S3

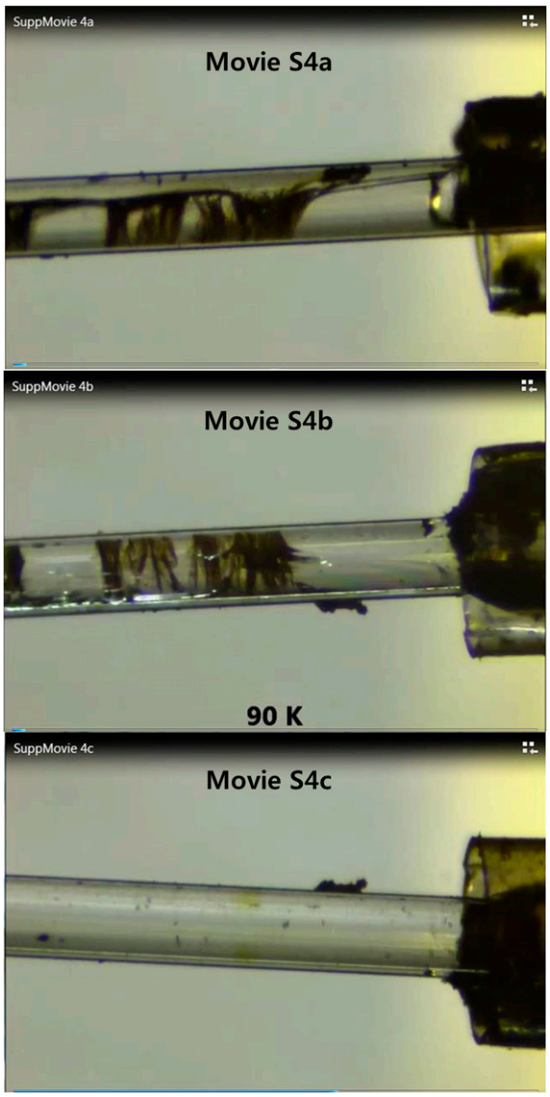

Movie S4. Crack healing in the HDA state of 1.5 M NaCl solution in a polycarbonate capillary. (*A*) The sample is rotated by 360° at 80 K to show cracks induced inside. The frame rate used for recording is 7.5 fps and video playback speed is 15 fps. (*B*) Crack healing inside the HDA sample during warming (from 80 to 160 K). Note that noticeable crack healing occurs above 115 K. The image frames are recorded every 5 K, and video playback speed is 2 fps. (*C*) The sample after warming. The sample is rotated by 360° at 160 K to show crack healing inside. Note that the cracks are completely healed.

Movie S4

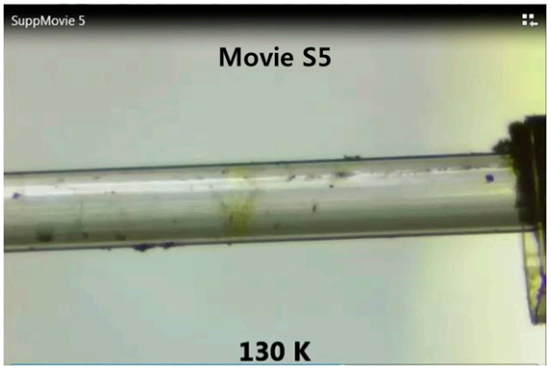

Movie S5. Crack healing in the HDA state of 1.5 M NaCl solution in a polycarbonate capillary during warming from 80 to 160 K (a different sample from that of Movie S4). Note that crack healing occurs noticeably above 120 K. The image frames are recorded every 5 K, and video playback speed is 2 fps.

Movie S5